

Hybrid nanocomposite by solid-solid reaction

Amel Ben Othman, Fadhila Ayari*, Malika Trabelsi Ayadi

Laboratoire des Applications de la Chimie aux Ressources et Substances Naturelles et à l'Environnement (LACReSNE),
Faculté de Sciences de Bizerte, Université de Carthage, Zarzouna 7021, Tunisia, Tel. +21621791747;
emails: fadhilaayari@yahoo.fr (F. Ayari), benothman_amel@yahoo.fr (A.B. Othman), malika.trabelsiayadi@gmail.com (M.T. Ayadi)

Received 6 April 2018; Accepted 20 October 2018

ABSTRACT

In order to synthesize nanocomposite hybrid material clay-calixarene by solid-solid reaction, calixarenic derivative (dicalixarenic amide derivative) has been synthesized, and the complexing properties have been studied. This calixarene has shown a high efficacy as a specific ionophore following the study of these complexing properties with respect to different metal cations with various toxicities. Results show a significant selectivity toward mercury. Natural Tunisian clay was purified and characterized by various methods such as X-ray diffraction, X-ray fluorescence, infrared spectroscopy, and transmission electron microscope. Intercalation of the calixarene in the interlayer space of the clay was confirmed by the increase of the basal space after reaction. Also, the comparison of the infrared spectra shows that the reaction has indeed taken place. Prepared nanocomposite has developed a high specific surface. This is the first synthesis of clay-calixarenic hybrid obtained by solid reaction, with the aim of respecting the environment as much as possible. Taking into account the calixarenic structure, it is assumed that the Ar-Cx hybrid is classed among the class I hybrids.

Keywords: Nanocomposite; Clay; Hybrid; Solid-solid reaction; Calixarene

1. Introduction

Nowadays, hybrid nanocomposite materials were widely used in various fields [1,2]. To ensure the best conditions to obtain these nanocomposites, the main criteria needs to be taken into account is the choice of organic and inorganic phases. Calixarene has become one of the most functionalizable macromolecules, adjustable according to the desired and flexible needs. It is relatively easy to prepare, ionophores with interesting selectivity, and has the possibility of decomplexing, but expensive. Hence, it cannot allow their use in pure form in environmental applications. It would be better to think of using them to develop materials, usable in thin layers, as a reusable and durable filter. The support, which could be used with this organic compound, should be abundant,

natural, inexpensive medium with exciting properties in the environmental field. For these reasons, clay has been chosen in this study.

Prepared materials, combining an organic phase and another inorganic phase, would be hybrid materials, and specifically, argilo-calixarenic hybrids are rarely synthesized so far and never by solid route. This type of versatile material is used in a wide range of applications such as optics [3–6], electronics [3,4], mechanical [3–5,7,8], environment [3,4,9], biology [3–5,10], and medicine [3–5].

The purpose of this work is to report the formation and characterization of hybrid materials, also called nanocomposites, clay-calixarene, through solid-solid reaction by mechanical grinding in the solid state of all compounds at room temperature.

* Corresponding author.

2. Experimental Section

2.1. Materials and reagents

Clay sample used in this work is a natural smectite (AB-b), extracted from a soil of "Ain Berda" situated in the north-east of Tunisia. This material was previously crushed and sieved to reduce a particle size and then underwent a purification stage, with Na_2CO_3 , according to the process described in this work [11]. Purified clay (Ab-p) is finally dried at 70°C and then crushed and sieved.

All reagents were of analytical grade and used without further purification: monomethyl ester calyx[4]arène, diéthylène triamine, methanol, toluène, dichlorométhane, hydrochloric acid, and Na_2CO_3 .

2.2. Preparation of clay-calixarenic hybrid

2.2.1. Synthesis of dicalixarenic derivative 2

The derivative dicalix 2 was prepared following a previously described procedure [12] via this reaction scheme (Fig. 1a).

In a 100-ml flask, monomethyl ester calyx[4]arène 1 was introduced with 0.3 of diethylène triamine and methanol/toluène: (1/1). This mixture was taken under reflux for 6 d under nitrogen atmosphere. After total evaporation

of solvents, the reaction residue is solubilized in the minimum of dichlorométhane and the product 2 is purified by chromatography on a silica column ($\text{CH}_2\text{Cl}_2/\text{acetone}$: 85/15). Obtained product has a white color with a yield of 48%.

2.2.2. Synthesis of clay-calixarenic hybrid

Clay-calixarenic nanocomposite was synthesized at room temperature through solid-solid reaction according to the method described in the previous work [13]. The mixtures of organic and inorganic phases were grinded manually using an agate mortar. The grinding time ($t_i \leq 10$ min) and the relative proportions were taken into consideration. Hereafter, the prepared materials were washed with the appropriate solvent to remove the excess of calyx absorbed in the clay surface. Total elimination was checked by the absence of the characteristic peaks of the calyx molecule in the UV-visible spectrum of the washing solution.

Synthesized nanocomposites were labeled Ar-Cx.

2.3. Characterization and analytical techniques

Composition of the clay sample was identified by X-ray diffractometer (XRD), and analysis was carried out using a PAN analytical X'Pert High Score Plus diffractometer, CuK_α radiation. Chemical composition of both samples was

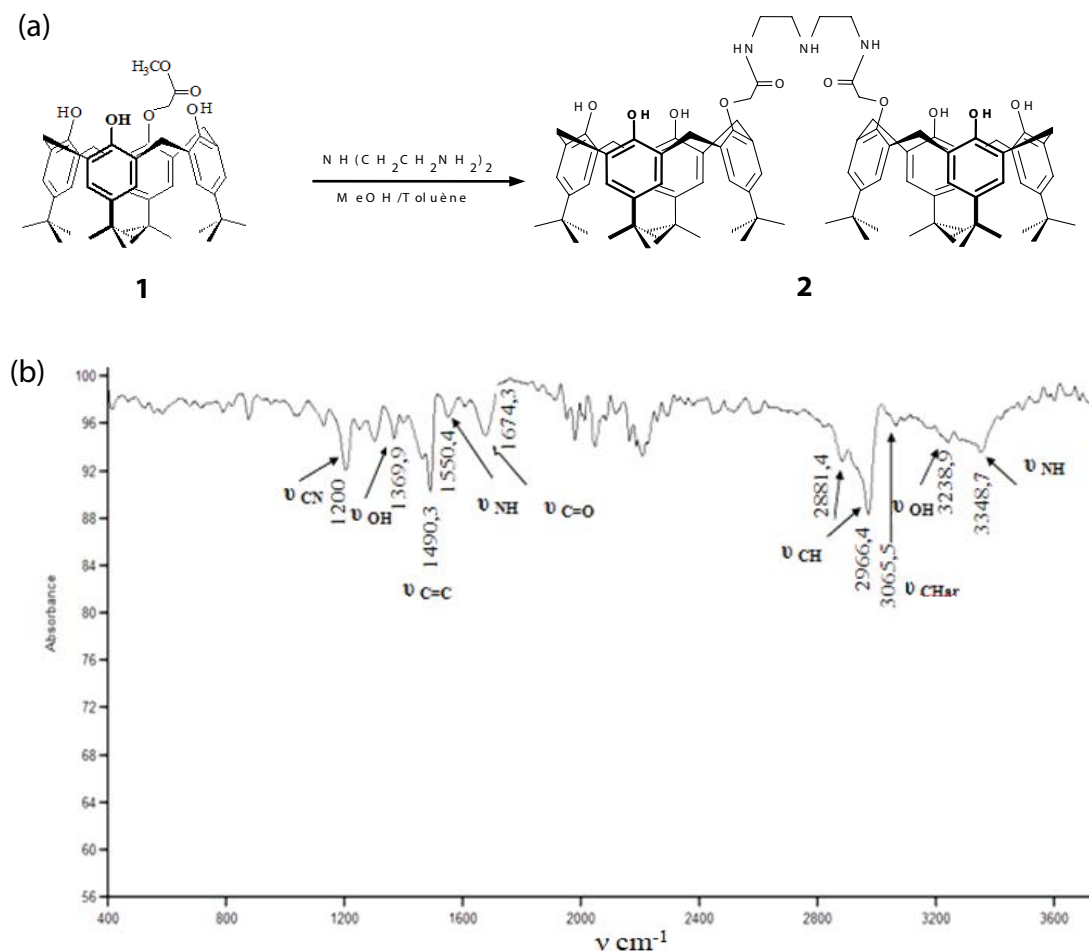


Fig. 1. (a) Synthesis of derivative dicalix 2; (b) infrared spectrum of calixarenic derivative 2.

investigated by X-ray fluorescence (XRF) spectrometer. Also, the composition of ArP sample was confirmed with EDX system. Cation exchange capacity (CEC) of raw and purified clay was estimated as described in previous studies [14]. Clay morphology was given by transmission electron microscopy (TEM). BET surface area (S_{BET}) and pore volumes of all samples were measured using the physical adsorption of nitrogen by Quantachrome Autosorb-1 instrument. The Fourier transform infrared spectra were acquired on a Perkin Elmer 783 dispersive spectrometer in the range of 4,000–400 cm^{-1} .

Atomic absorption spectroscopy (AAS) was used to quantify the release ions from clay sample.

UV-visible spectrophotometer (Shimadzu Model Perkin Elmer) was used to investigate the complexing properties of dicalixarenic derivative 2.

3. Results and discussion

3.1. Properties of dicalixarenic derivative 2

3.1.1. Structural data

Structural data and geometric presentation of dicalixarenic derivative are presented in the following table (Table 1).

Due to the flexibility of the calixarene molecules, their thickness can vary between two values depending on whether this thickness is perpendicular to their maximum or minimum surface.

3.1.2. Infrared spectroscopy

The infrared absorption spectrum of the calixarenic derivative involved in this study is presented in Fig. 1b. The main absorption bands are summarized in Table 2.

Table 1
Geometric description of dicalixarenic derivative

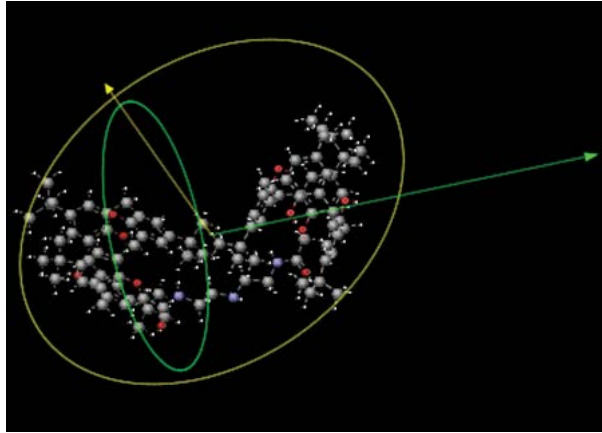
Geometric description	Value	Geometric presentation
Minimum projection area	170.59	
Maximum projection area	273.64	
minimum projection radius	9.19	
maximum projection radius	14.06	
length perpendicular to the maximum surface	17.74	
length perpendicular to the minimum surface	28.01	
Van Der Walls volumew	1,487.02	

Table 2
The main absorption bands of calixarenic derivative

Vibration mode	Elongation	Deformation
OH	A large and intense band around 3,400–3,200 cm^{-1} (OH with intermolecular hydrogen band)	Band around 1,410–1,330 cm^{-1}
N–H	A band with weak intensity situated in 3,400–3,300 cm^{-1}	A second band situated around 1,570–1,510 cm^{-1}
C–H aromatic	A band with average intensity appears around 3,080–3,030 cm^{-1}	Bands situated between 900 and 700 cm^{-1}
C–H methyl group	<ul style="list-style-type: none"> Asymmetric: a band with high intensity around 2,925 cm^{-1} Symmetric: a band with average intensity around 2,870 cm^{-1} 	<ul style="list-style-type: none"> Asymmetric: a band with average intensity around 1,460 cm^{-1} Symmetric: a band at 1,380 cm^{-1}
C–N amines	A band with average intensity in the region 1,230–1,030 cm^{-1}	Bands around 700–400 cm^{-1} , deformation out of the plane of aromatic nucleus.
C=C aromatic	A band with variable intensity situated around 1,500 cm^{-1}	
C=O (secondary amide group)	A band with high intensity situated in the region 1,700–1,630 cm^{-1}	
C=O ester	A band with high intensity in the region 1,750–1,730 cm^{-1}	
C–O ester	Two bands with high intensity situated in the region 1,300–1,050 cm^{-1}	

3.1.3. Study of the complexing properties of calixarenic derivative 2

The study of the complexing properties of calixarenic derivative 2 (ligand) was investigated, in acetonitrile, with the following cations: Ni^{2+} , Cu^{2+} , Al^{3+} , and Hg^{2+} using UV-visible spectrophotometer. The complexation was carried out by direct titration in the spectrophotometric tank, and the spectra of the different complex solutions were recorded in the UV range between 230 and 340 nm.

The formation of a new species is achieved by modifications of the ligand spectrum such as hypochromic or hyperchromic effect, hypsochromic or bathochromic displacement of the bands, or the appearance of isobestic points.

In this work, we give only the UV-visible spectra relating to the complexation of mercury by the calixarenic derivative 2 (Fig. 2).

Stability constants of the complexes of the studied systems in acetonitrile are presented in Table 3.

The recorded spectral variations are interpreted by the formation of mononuclear complexes with all cations and binuclear in addition to ML with nickel and copper. From the point of view of ionic radius, Al^{3+} is smaller than Ni^{2+} and Cu^{2+} , and on the other hand, Hg^{2+} is larger; so the appearance of the species M_2L can only be interpreted by the adequacy between the size of the calixarenic cavity and the ionic radius of Ni^{2+} and Cu^{2+} . By plotting the stability profiles, we obtain Fig. 3.

According to Fig. 3, it can be noted that the derivative 2 has selectivity for Hg^{2+} where $\text{Hg}^{2+}/\text{Al}^{3+}$ is 270 times.

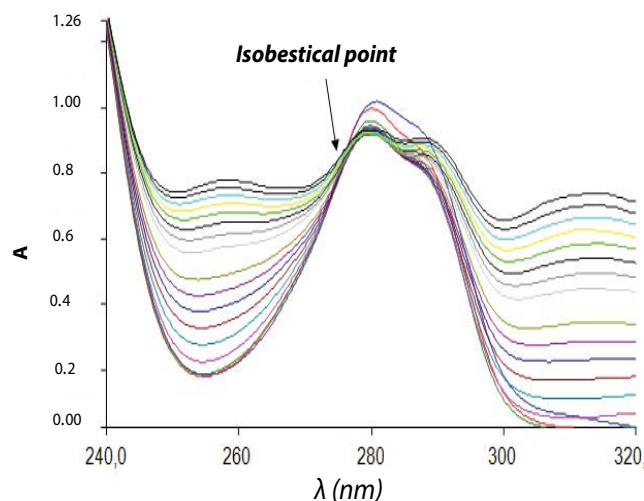


Fig. 2. Hg^{2+} complexation with calixarenic derivative 2 in acetonitrile ($0 \leq R_{\text{M/L}} \leq 4.5$) and at 20°C , $C_L = 5 \times 10^{-5}\text{M}$.

Table 3

Stabilities of cation metallic complexes ($\log K_{11}$) with calixarenic derivative 2 in acetonitrile

	M:L	Ni^{2+}	Cu^{2+}	Al^{3+}	Hg^{2+}
Calixarenic derivative 2	1:1	4.67 ± 0.04	5.07 ± 0.01	4.39 ± 0.02	6.82 ± 0.02
	2:1	7.20 ± 0.19	8.54 ± 0.19	–	–

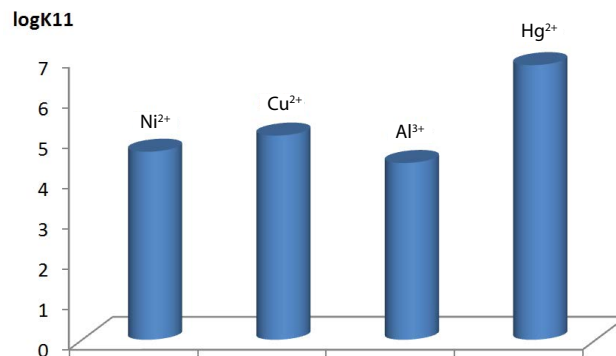


Fig. 3. Formed ML complex stabilities with derivative 2.

3.2. Characterization of clay sample

3.2.1. X-ray diffraction

XRD measurements of both clay samples before and after purification are presented in Fig. 4a. It can be seen that natural clay (AB-b) contains many impurities such quartz (3.34 Å; 4.27 Å) and calcite (3.03 Å), which disappear after purification [15]. The signal d_{001} of AB-b at 15.3 Å confirms the smectitic nature of this clay which was shifted to 12.38 Å after purification.

3.2.2. Infrared spectroscopy

Infrared spectrums of raw and purified samples are shown in Fig. 4b. As can be seen, the band between 1,600 and 1,700 cm^{-1} can be attributed to the valence vibrations of the OH group of the water. The band between 3,200 and 3,800 cm^{-1} corresponds to the elongation vibrations of the internal OH groups. The Si–O bond is characterized by the intense band located between 900 and 1,200 cm^{-1} and, centered at 1,020 cm^{-1} , corresponds to the valence vibrations of the Si–O bond [16], to the Si–O–Al bond extension vibrations, and to hydroxyls perpendicular to the surface (translational OH) [17].

3.2.3. Thermal analysis

ATD-ATG thermograms relating to samples AB-b and AB-p are given, respectively, in Figs. 5a and b.

3.2.3.1. Thermogravimetric analysis

Thermogram of the raw sample AB-b (Fig. 5a) has two peaks between 95°C and 133°C corresponding to the departure of the interlayer water and the loss of moisture

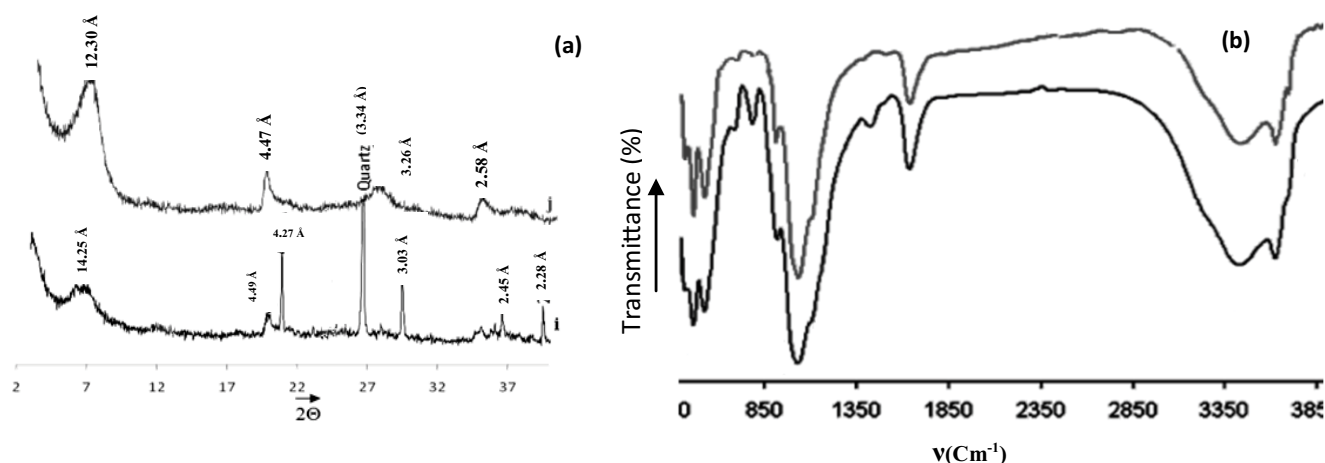


Fig. 4. (a) X-ray diffractograms and (b) IR spectra of AB-b (i) and AB-p (j)

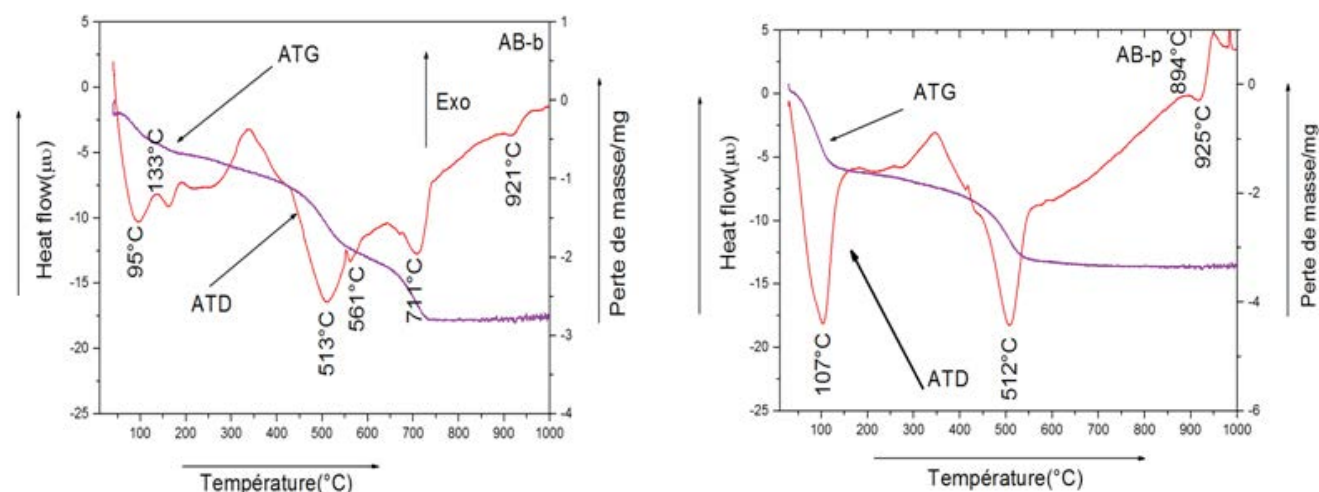


Fig. 5. (a) ATD-ATG of raw clay AB-b and (b) ATD-ATG of purified clay AB-p.

water. An endothermic peak of high intensity was located at 513°C due to the clay dehydroxylation. This probably indicates the presence of a beidellitic character or the presence of smectite-illite inter-stratification. The peak at 561°C is relative to the decarbonation of the clay. The thermogram of the purified sample AB-p (Fig. 5b) shows an endothermic peak at 107°C due to the loss of interfoliar water and a peak at 512°C relative to the dehydroxylation of the purified clay.

3.2.3.2. ATD

Thermogravimetric analysis curves make it possible to follow the mass loss of the sample. These curves represent three mass losses for the raw clay and two losses for the purified clay. The first loss of mass is between 100°C and 130°C, corresponding to the loss of moisture and interfoliar water. The second loss of mass at 513°C and 512°C corresponds to the loss of constitution water. The third loss of mass occurs at 561°C and corresponds to the decarbonation of the clay [15].

This loss appears only on the thermogram of the AB-b raw clay. The loss percentages of constitution water and hydration are illustrated in Table 4.

3.2.4. X-ray fluorescence

The chemical analysis makes it possible to know the composition of the clay as well as the nature of these interfoliar cations. The percent compositions expressed as oxides of the major elements contained in the raw and purified clay were determined using an XRF spectrometer (Table 4).

According to this analysis, it can be concluded that

- The ratio $\text{SiO}_2/(\text{Al}_2\text{O}_3 + \text{Fe}_2\text{O}_3 + \text{MgO})$ close to 2, it is then a phyllosilicate 2/1, dioctahedral of the group of smectites,
- The CaO content passes after purification from 12.820 to 0.106,
- K_2O content increases after purification which inspires the existing small fraction of illite in the studied clay network.

Table 4
Physicochemical characterization and CEC of raw and purified clay

Samples	Loss of hydration water (%)			Loss of constitution water (%)					
AB-b	2.24			4.097					
AB-p	6.522			5.261					
Chemical composition									
	SiO ₂	Al ₂ O ₃	Fe ₂ O ₃	CaO	MgO	Na ₂ O	K ₂ O	PF	CEC
AB-b	59.4	13.83	6.69	12.82	0.81	0.66	0.83	15	43.35
AB-p	54.15	17.67	5.88	0.11	0.95	1.38	1.25	16	89

3.2.5. Cation exchange capacity

The measurements of the CECs of the clays studied are determined by the method of MANTIN [14]. Obtained results are given in Table 4. It should be noted that for the raw sample AB-b, the CEC (43.35 meq/100 g of calcined clay) is almost half that of the purified sample (89 meq/100 g of calcined clay). This difference is due to the presence of impurities in the untreated sample, which are eliminated almost completely after purification.

Obtained CEC values are characteristic of smectitic clay.

3.2.6. Transmission electron microscopy

The use of TEM has been done in order to complete the mineralogical characterization and to determine the clay morphology [18]. The observation of the cliché obtained by TEM of the purified clay clearly shows the sample sheet structure (Fig. 6). The thickness of the sheet is 12.39 Å, which is in good agreement with the XRD analysis.

The semiquantitative analysis provided by the EDS energy dispersive X-ray micro-analysis (EDAX probe) makes it possible to estimate the atomic percentages in major elements contained in the purified sample (Fig. 6). These results confirm those of the chemical analysis and also show the existence of sodium (inter-ionic cation), which reflects that the sodium exchange took place.

3.2.7. Granulometric analysis

The particle size analysis of the AB-b sample powder was carried out by laser granulometry in aqueous suspension. The method consists in taking a volume of an aqueous suspension of the sample, which will be dispersed in the column of the apparatus. The sample was measured three times with a time interval of 10 s and a measurement time of 60 s. The granulometric distribution curve of this clay (Fig. 7) shows a

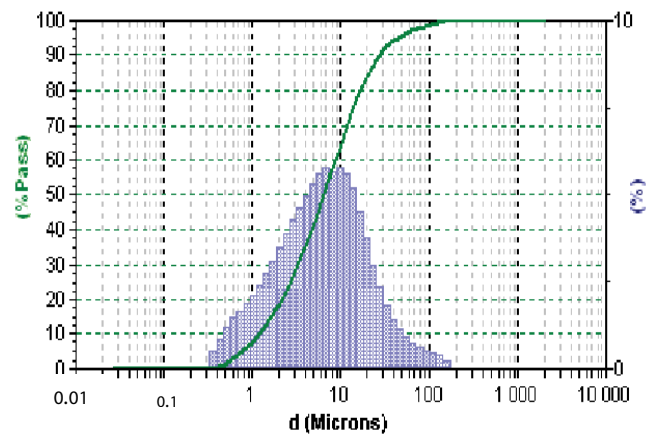


Fig. 7. Granulometric distribution of AB-p.

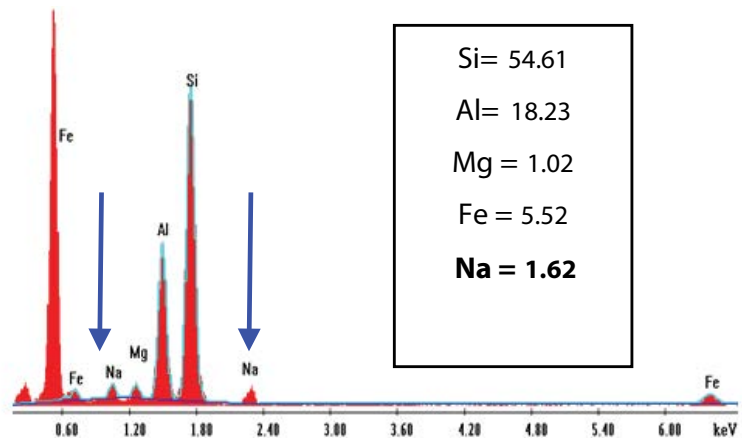
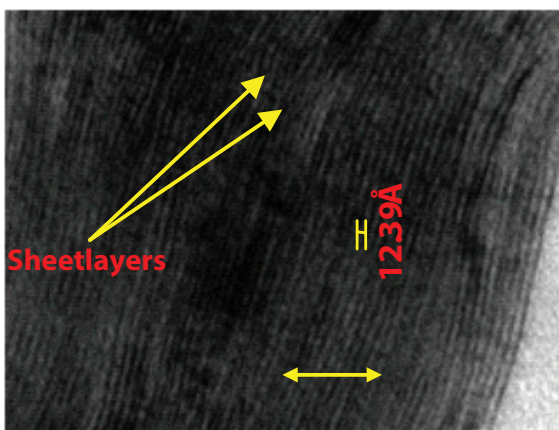


Fig. 6. TEM analysis and EDS spectrum of AB-p.

distribution with a single population. This Gaussian pace has a maximum around 10 μm. This shows the fineness of the grains of the AB-p sample.

3.3. Effect of grinding time

3.3.1. X-ray diffraction analysis

Solid-state intercalation of organic compounds in the interfoliar space of the clay mineral consists of grinding the reagents at room temperature. Therefore, it is necessary to study the effect of grinding time on the clay structure. Fig. 8 shows X-ray diffractograms of different samples crushed for a grinding time interval varying from 2 to 25 min.

Results show that the signal $d_{001} = 12.3 \text{ \AA}$ expanded more and more with the increase of the grinding time and becomes more extensive. On the other hand, the signal d_{002} disappears after 25 min of grinding. These two findings suggest that the grinding force predominates essentially in the perpendicular direction of the clay layers. This causes a slippage of the clay sheets. Obtained results were in agreement with previous works [19–24].

After 25 min of grinding, a wide band appears in a 2θ range $\in [15^\circ\text{--}30^\circ]$ indicating the formation of the amorphous silica due to the effect of the clay structure destruction. Also, it should be noted that the parameter c of the crystalline mesh decreases as a function of the grinding time. The intensity of $hk0$ signal decreases, but their position remains unchanged.

First studies about the effect of the grinding time on clay minerals date to 1930; Kelly et al. [25–27] reported that grinding natural and purified montmorillonite for 72 h increases significantly the CEC of the clay. Authors concluded that this increase is due to the appearance of new active sites after grinding.

Contrary to these observations, it has been reported that the grinding has no effect on the crystalline structure of the clay [23]. The effect of the grinding decreases with the increase of the crushed quantity. In our case, we tried to get as close as possible to the operating conditions of nanocomposite synthesis; for this reason, we carried out this study with an amount of clay well chosen to avoid the effect of grinding.

3.3.2. Atomic absorption spectroscopy

The effect of grinding on the clay structure was followed by the quantification of release ions. So, various ground samples were washed by a weakly acidic solution in order to release these dissolved cations. The percentages of released Fe^{2+} , Mg^{2+} , and Al^{3+} ions are estimated by AAS (Table 5). Results show that prolonged grinding can lead to the release of clay structural ions. These results confirm those obtained by XRD.

3.3.3. Textural study and morphology

The textural and morphological study of the crushed samples was carried out by BET for a grinding time

Table 5
Percentage of Fe^{2+} , Al^{3+} , and Mg^{2+} ions released from crushed clay

M_xO_y t_i (min)	Fe_2O_3	Al_2O_3	MgO
t_0	0	0	0
t_2	2	1.25	3
t_5	2.2	5	3
t_{10}	7	11	5
t_{15}	13	15	12
t_{25}	28	20	25

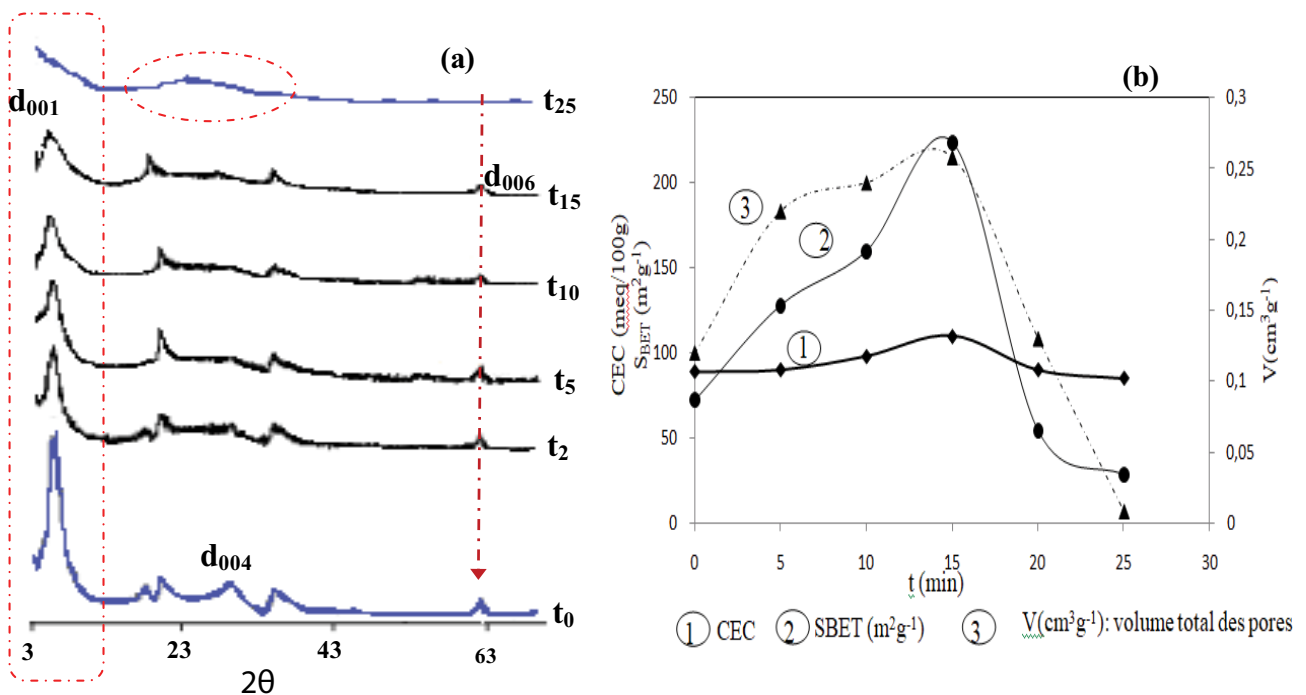


Fig. 8. (a) XRDs and (b) textural properties of different samples after grinding vs time (t_i (min); $i \in [0\text{--}25]$).

$t \geq 10$ min since the XRD monitoring of the crushed samples does not show a significant change even after 15 min of grinding.

Results show an increase in the adsorbed nitrogen volume for P/P_0 values greater than 0.1 under the effect of grinding, probably due to the reduction in particle size of the clay during the milling process. Grinding and increasing the space between particles creates pores of large diameters. However, a prolonged period of grinding has the effect of agglomeration of clay particles, as well as a decrease in nitrogen adsorption. The nitrogen adsorption/desorption isotherms exhibit H4-type hysteresis according to the classification of BRUNAUER, EMMETT, and TELLER [28], characterizing solids with slotted pores. Fig. 9 shows the textural properties of the ground samples: the specific surface, the pore volume, and the CEC. These parameters increase linearly with the grinding time for treatment periods of less than 10 min, reaching a maximum after grinding for 15 min: CEC (110 meq/100 g), S_{BET} ($224 \text{ m}^2 \text{ g}^{-1}$), and V ($0.258 \text{ cm}^3 \text{ g}^{-1}$). A gradual decrease of these parameters beyond this grinding period is reported.

To conclude, it seems that the first 15 min of grinding leads to an increase in the specific surface area and the CEC, as well as an increase in the pore diameters, whereas beyond this period, the properties of adsorption decrease. These results explain the observations of Yariv and his collaborators [29] concerning the solid-state intercalation of phenol in montmorillonite. They observed that during the first minutes of grinding, the adsorption capacity of phenol by the clay increases, and then it undergoes a decrease. The authors have not given an interpretation of this observation, but we can say that this is due essentially to the effect of grinding on the structure of the clay.

3.4. Characterization of hybrid clay-calixarenic

3.4.1. Infrared spectroscopy

The IR spectrum of the prepared clay-calixarenic sample is presented in Fig. 10. IR spectrum of purified clay (AB-p) and calixarene were presented for comparison. As can be seen, intercalation of the calixarenic derivative is confirmed

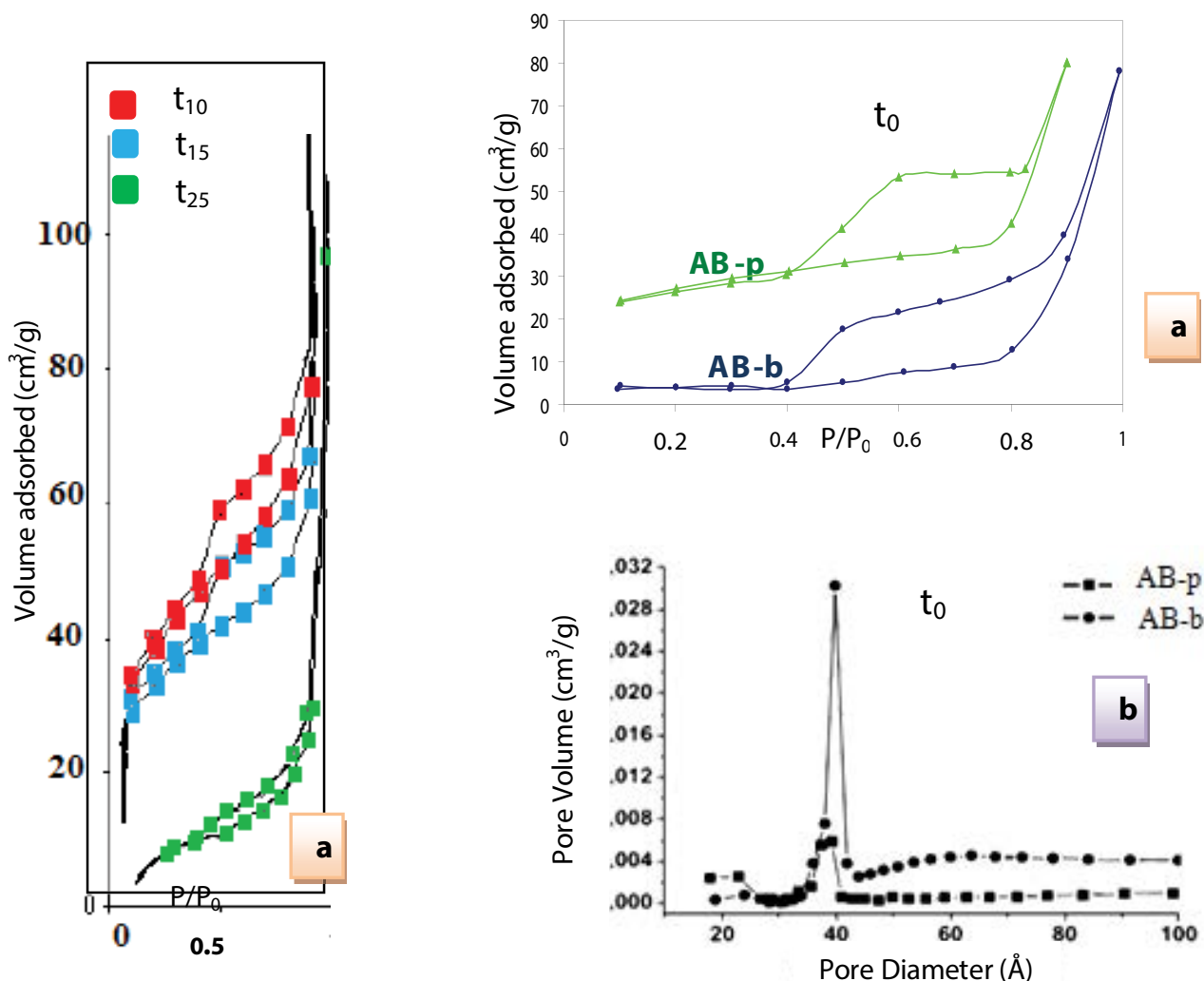


Fig. 9. (a) Nitrogen adsorption-desorption isotherms of different samples as function of grinding time and (b) pore size distribution for AB-p and AB-b.

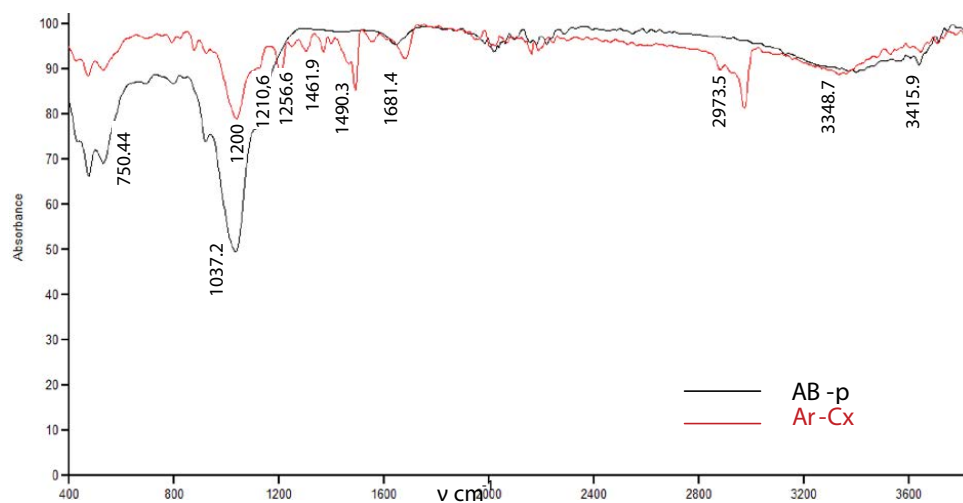


Fig. 10. IR spectrum of AB-p and Ar-Cx.

by the appearance of the bands characteristic of the adequate functional groups of calixarene.

The passage of the free calixarene to the hybrid caused the attenuation of all calixarene derivative bands such as the band relating to the elongation ($3,400\text{--}3,200\text{ cm}^{-1}$) and the deformation vibration ($1,410$ and $1,330\text{ cm}^{-1}$) of phenolic OH; valence ($3,080\text{--}3,030\text{ cm}^{-1}$) and deformation ($900\text{--}700\text{ cm}^{-1}$) bands of aromatic C–H; the asymmetric ($2,925\text{ cm}^{-1}$) and symmetrical ($2,870\text{ cm}^{-1}$) elongation band as well as the asymmetric ($1,460\text{ cm}^{-1}$) and symmetrical ($1,380\text{ cm}^{-1}$) strain of the C–H methyl groups; the vibration band ($1,500\text{ cm}^{-1}$) and deformation vibration bands out of the plane ($700\text{--}400\text{ cm}^{-1}$) of (C=C) arom of the aromatic ring. In addition, we also notice the appearance of the vibration bands of the silicate anion. These attenuated calixarene bands were added (or overlapped) to those of the clay to form the hybrid spectrum.

3.4.2. X-ray diffraction analysis

Diffraction patterns of the purified clay and the hybrid nanocomposite are shown in Fig. 11. Results show that the d_{001} basal spacing of different samples appears at variable positions after introduction of calixarene. The increase of the signal d_{001} , compared with that of the starting purified clay, proves the success of the intercalation of the molecule in the interfoliar space of the clay and the formation of a hybrid Ar-Cx material. Taking into account the thickness of a clay sheet, which is equal to 9.6 \AA , the spacing of interlamellar space ($\Delta d = d_{001} - 9.6$) could be calculated for the hybrid (Table 6).

The bibliographical analysis on the state of arrangement of organic molecules in the interfoliar space will make it possible to estimate the nature of arrangement of the calixarene macrocycles in the interlamellar space. The arrangement of organic molecules in the interfoliar space of clay has been studied for the first time by Hofman and Brindley [30]. Two main types of scheme are reported:

- An arrangement parallel to the direction of the sheets: in which the chains of the molecule are extended parallel

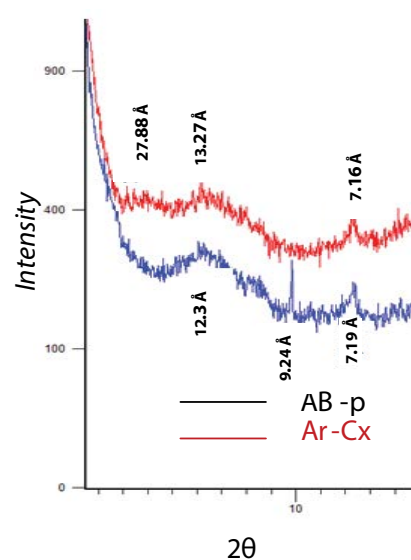


Fig. 11. X-ray diffractogram of hybrid nanocomposite Ar-Cx and AB-p.

Table 6
Interfoliar spacing value of the hybrid Ar-Cx

	AB-p	Ar-Cx
d_{001} (Å)	12.3	27.88
$\Delta d = d_{001} - 9.6$ (Å)	2.7	18.28

to the sheets of the clay by forming a configuration in monolayer or bilayer.

- An arrangement in a direction inclined or perpendicular to the layers of the clay.

Based on the dimensions of the different calixarenes used in this investigation (calculated taking into account Van

der Waals radius, covalent binding distance, and binding angle), on the XRD results, and on the organic compounds interposed in the interfoliar space of the clays by forming a parallel, perpendicular, or inclined arrangement in the direction of the mineral leaflets, furthermore, they may form a single layer, two layers, or more layers. We were able to estimate the state of arrangement of each calixarene. Because of the flexibility of the calixarenic molecules, their thickness can vary between two values depending on whether this thickness is perpendicular to their maximum or minimum surface. The spacing of the basal line is substantially

equal to the minimum thickness possible of the appropriate calixarenic derivative. We can therefore estimate that the calixarene molecules flatten in a flattened manner parallel to the clay sheets forming a single layer with a slight inclination. In the figure below (Fig. 12a), we give, for explanatory purposes, an estimated schematic representation of the intercalation of calixarenic molecules during the formation of the hybrid Ar-Cx.

It is well known that surface charge is among the fundamental property of clays. The main origin of this surface charge comes from isomorphous substitutions within the

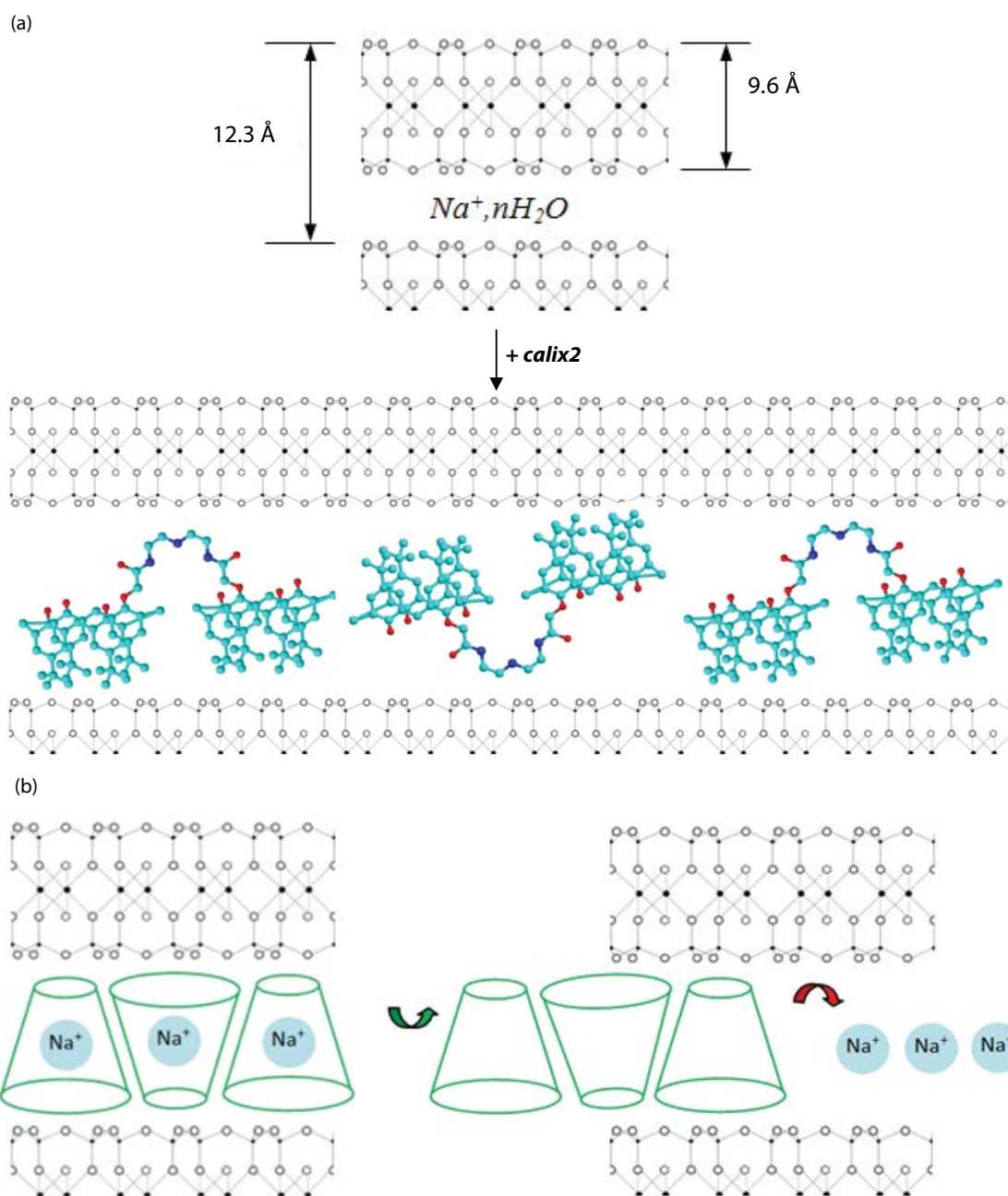


Fig. 12. (a) Schematic representation of calixarene arrangement in the clay interlayer; (b) Estimation of the exchange reaction between calixarene and interfoliar cations (substitution or complexation).

crystal lattice. This negative charge is the commonly noted permanent structural load (σ_0) [31] and is around $7 \times 10^{-3} e \text{ \AA}^{-2}$.

The origin of the second charge that depends on the pH (note σ_H) comes from the presence of oxides or hydroxyl groups of silanol ($-\text{SiOH}$) and aluminol ($-\text{AlOH}$) types. These hydroxyl groups, present at the edges of the clay surfaces (Fig. 13), admit an amphoteric character following the reactions:

(S = Al ou Si)

It should be noted that the clay sample develops a negative surface charge considering pH of the zero charge point of the clay used, an average of 6.5, and the pH of an aqueous solution containing the clay in question having a value of 5.7.

3.4.3. Textural study by BET

The S_{BET} and pore volume of AB-p and Ar-Cx (having the highest basal spacing according to XRD analysis) are determined and presented in Table 7. The adsorption and desorption isotherms of the nitrogen of Ar-Cx are illustrated in Fig. 14. The isotherm is of type (II) having a hysteresis loop type H4, with a delay in desorption (denoted by an opening of the loop at low pressure level) probably due to the trapping of nitrogen molecules by calixarene molecules. A considerable increase in the S_{BET} for the Ar-Cx sample is noted ($2,898 \text{ m}^2 \text{ g}^{-1}$) compared with the starting sample ($72 \text{ m}^2 \text{ g}^{-1}$). The total volume of the clay-calixarene hybrid largely decreases, due to the fact that the interparticle pores of the bentonite are sheltered by the calixarene molecules, which induces an inhibition of the passage of the N_2 molecules at the surface reaction sites.

From the textural and XRD analysis and those of the IR spectroscopy, it can be noted that the process of intercalation

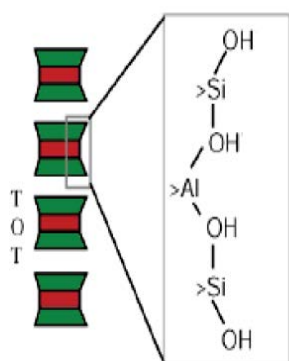


Fig. 13. Silanol ($-\text{SiOH}$) and aluminol ($-\text{AlOH}$) groups at the edges of clay surface type 2:1.

Table 7

BET (S_{BET}) surface area and pore volumes of AB-p and Ar-Cx total volume à $P/P_0 = 0.96$ (V_{tot}) and Pore diameter D (Å)

Samples	S_{BET} ($\text{m}^2 \text{ g}^{-1}$)	Pore diameter D (Å)	V_{tot} ($\text{cm}^3 \text{ g}^{-1}$)
Ar-Cx	2,898.07	15.638	0.08
AB-p	72	18	0.12

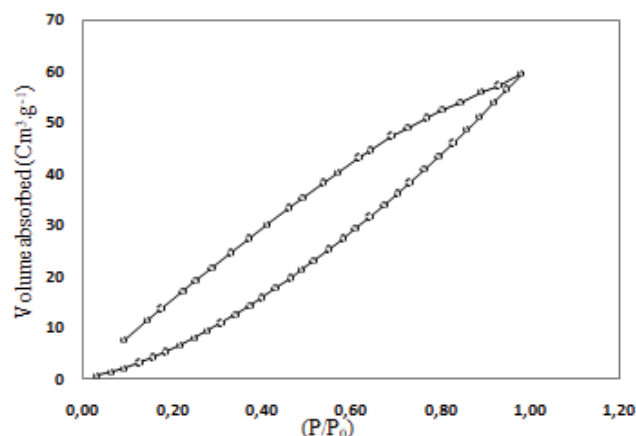


Fig. 14. Nitrogen adsorption-desorption isotherm of Ar-Cx.

was successful and is based mainly on a phenomenon of cation exchange and surface adsorption.

4. Conclusion

All the work done in this study is part of the development of new inorganic-organic hybrid materials based on clay and calixarene. The choice of clay being justified, among others, because it is naturally abundant and not expensive, with attractive adsorption properties and a possibility of re-release. The choice of calixarenes was supported by their complexing and extracting properties adjustable to the finalities according to their functionalization, their particular selectivity vis-a-vis ionic entities or not even at concentrations of the order of a micrometer, as well as the possibility of decomplexation therefore of reuse. Since their cost does not allow pure use, dispersion in an inorganic matrix would be a solution to access the properties of the two components and even to the new properties characterizing the new nanocomposite.

From the results obtained, we can affirm the success of intercalation of the calixarene derivative in the interfoliar space by a separation of the basal space and a significant increase of the specific surface. Taking into account the calixarene structure, the classification of the Ar-Cx hybrid, with the benzenes providing the β - β type bonds and the hydroxides favoring hydrogen bonds, is assumed among the class I hybrids.

Hybrid nanocomposite could contribute significantly in the environmental field by a quaternary treatment of treated water or a specific treatment of water for medicinal use.

References

- [1] A. Malinauskas, Chemical deposition of conducting polymers, *Polymer*, 42 (2001) 39–59.
- [2] R.F. De Farias, C. Airolidi, Synthesis and characterization of an VOPO_4 -polyaniline lamellar hybrid compound, *Solid State Sci.*, 5 (2003) 611.
- [3] C. Sanchez, B. Julian, P. Belleville, M. Popall, Applications of hybrid organic-inorganic nanocomposites, *J. Mater. Chem.*, 15 (2005) 3559.
- [4] C. Sanchez, P. Belleville, M. Popall, L. Nicole, Applications of advanced hybrid organic-inorganic nanomaterials: from laboratory to market, *Chem. Soc. Rev.*, 40 (2011) 696.

- [5] L. Nicole, L. Rozes, C. Sanchez, Integrative approaches to hybrid multifunctional materials: from multidisciplinary research to applied technologies, *J. Adv. Mater.*, 22 (2010) 3208.
- [6] K.C. Krogman, T. Druffel, M.K. Sunkara, Anti-reflective optical coatings incorporating nanoparticles, *Nanotechnology*, 16 (2005) S338.
- [7] V.A. Soloukhin, W. Posthumus, J.C. Brokken-Zijp, J. Loos, Mechanical properties of silica–(meth) acrylate hybrid coatings on polycarbonate substrate, *Polymer*, 43 (2002) 6169.
- [8] E. Barna, B. Bommer, J. Kursteiner, A. Vital, V.O. Trzebiatowski, W. Koch, B. Schmid, T. Graule, Innovative, scratch proof nanocomposites for clear coatings, *Composites Part A*, 36 (2005) 473.
- [9] S. Takahashi, H.A. Goldberg, C.A. Feeney, D.P. Karim, M. Farrell, K. O'Leary, D.R. Paul, Gas barrier properties of butyl rubber/vermiculite nanocomposite coatings, *Polymer*, 47 (2006) 3083.
- [10] G. Schottner, K. Rose, U. Posset, Scratch and abrasion resistant coatings on plastic lenses—state of the art, current developments and perspectives, *J. Sol-Gel Sci. Technol.*, 27 (2003) 71.
- [11] S. Khelifi, F. Ayari, A. Choukchou-Braham, D.B.H. Chehimi, The remarkable effect of Al–Fe pillaring on the adsorption and catalytic activity of natural Tunisian bentonite in the degradation of azo dye, *J. Porous Mater.*, 25 (2018) 885–896.
- [12] A.B. Othman, Y.H. Lee, K. Ohto, R. Abidi, Y. Kim, J. Vicens, Multi-calixarenes with multidentate coordination sites, *J. Inclusion Phenom. Macrocycl. Chem.*, 62 (2008) 187.
- [13] N. Khaorapong, M. Ogawa, Solid-state intercalation of 8-hydroxyquinoline into Li (I)-, Zn (II)-and Mn (II)-montmorillonites, *Appl. Clay Sci.*, 35 (2007) 31.
- [14] I. Manton, Accounts of the sessions of the academy of sciences, Series D: Natural sciences, 269 (1969) 815.
- [15] F. Ayari, E. Srasra, M. Trabelsi-Ayadi, Characterization of bentonitic clays and their use as adsorbent, *Desalination*, 185 (2005) 391.
- [16] A. Aarfane, A. Salhi, M. Elkrati, S. Tahiri, M. Monkade, E.K. Lhadi, M. Bensitel, Kinetic and thermodynamic study of the adsorption of Red195 and Methylene blue dyes on fly ash and bottom ash in aqueous medium, *J. Mater. Environ. Sci.*, 5 (2014) 1927.
- [17] K.L. Konan, J. Soro, J.Y. Andji, S. Oyetola, G. Kra, Etude comparative de la déshydroxylation/amorphisation dans deux kaolins de cristallinité différente, *J. Soc. Ouest-Afr. Chim.*, 30 (2010) 29.
- [18] O. Touret, C.H. Pons, D. Tessier, Y. Tardy, Etude de la répartition de l'eau dans des argiles saturées Mg^{2+} aux fortes teneurs en eau, *Clay Miner.*, 25 (1990) 217.
- [19] R.L. Frost, J. Kristof, É. Makó, W.N. Martens, Modification of the hydroxyl surface of kaolinite through mechanochemical treatment followed by intercalation with potassium acetate, *Langmuir*, 18 (2002) 6491.
- [20] R.L. Frost, É. Makó, J. Kristof, J.T. Klopogge, Modification of kaolinite surfaces through mechanochemical treatment—a mid-IR and near-IR spectroscopic study, *Spectrochim. Acta, Part A*, 58 (2002) 2849.
- [21] É. Makó, R.L. Frost, J. Kristof, E. Horvath, The effect of quartz content on the mechanochemical activation of kaolinite, *J. Colloid Interface Sci.*, 244 (2001) 359.
- [22] R. Reynolds Jr, D. Bish, The effects of grinding on the structure of a low-defect kaolinite, *Am. Mineral.*, 87 (2002) 1626.
- [23] P.J. Sánchez-Soto, J.L. Pérez-Rodríguez, I. Sobrados, J. Sanz, Influence of grinding in pyrophyllite–mullite thermal transformation assessed by ^{29}Si and ^{27}Al MAS NMR spectroscopies, *Chem. Mater.*, 9 (1997) 677.
- [24] E. Mendelovici, Comparative study of the effects of thermal and mechanical treatments on the structures of clay minerals, *J. Therm. Anal. Calorim.*, 49 (1997) 1385.
- [25] W.P. Kelley, Calculating formulas for fine grained minerals on the basis of chemical analysis, *Am. Mineral.*, 30 (1945) 1.
- [26] W.P. Kelley, W.H. Dore, A.O. Woodford, S.M. Brown, The colloidal constituents of California soils, *Soil Sci.*, 48 (1939) 201.
- [27] W.P. Kelley, H. Jenny, S.M. Brown, Hydration of minerals and soil colloids in relation to crystal structure, *Soil Sci.*, 41 (1936) 259.
- [28] S. Brunauer, L.S. Deming, W.E. Deming, E. Teller, On a theory of the van der Waals adsorption of gases, *J. Am. Chem. Soc.*, 62 (1940) 1723.
- [29] S. Yariv, I. Lapidés, The effect of mechanochemical treatments on clay minerals and the mechanochemical adsorption of organic materials onto clay minerals, *J. Mater. Synth. Process.*, 8 (2000) 223.
- [30] R. Hoffmann, G. Brindley, Adsorption of non-ionic aliphatic molecules from aqueous solutions on montmorillonite, *Geochim. Cosmochim. Acta*, 20 (1960) 15.
- [31] F.H. Frimmel, The chemistry of soils, *Angew. Chem.*, 102 (1990) 463.